PHYSICAL REVIEW B **88**, 161107(R) (2013)

Conducting channel at the $LaAlO_3/SrTiO_3$ interface

Z. Huang,[1] X. Renshaw Wang,[1,2] Z. Q. Liu,[1,2] W. M. Lü,[1,3] S. W. Zeng,[1,2] A. Annadi,[1,2] W. L. Tan,[2] X. P. Qiu,[3] Y. L. Zhao,[1,2] M. Salluzzo,[4] J. M. D. Coey,[1,5] T. Venkatesan,[1,2,3] and Ariando[1,2,*]

[1]*NUSNNI-NanoCore, National University of Singapore, 117411 Singapore, Singapore*
[2]*Department of Physics, National University of Singapore, 117542 Singapore, Singapore*
[3]*Department of Electrical and Computer Engineering, National University of Singapore, 117576 Singapore, Singapore*
[4]*CNR-SPIN, Complesso MonteSantangelo via Cinthia, I-80126 Napoli, Italy*
[5]*School of Physics and CRANN, Trinity College, Dublin 2, Ireland*

(Received 24 February 2013; revised manuscript received 23 May 2013; published 24 October 2013)

Localization of electrons in the two-dimensional electron gas at the $LaAlO_3/SrTiO_3$ interface is investigated by varying the channel thickness in order to establish the nature of the conducting channel. Layers of $SrTiO_3$ were grown on $NdGaO_3$ (110) substrates and capped with $LaAlO_3$. When the $SrTiO_3$ thickness is $\leqslant 6$ unit cells, most electrons at the interface are localized, but when the number of $SrTiO_3$ layers is 8–16, the free carrier density approaches 3.3×10^{14} cm^{-2}, the value corresponding to charge transfer of 0.5 electrons per unit cell at the interface. The number of delocalized electrons decreases again when the $SrTiO_3$ thickness is $\geqslant 20$ unit cells. The ~ 4 nm conducting channel is therefore located significantly below the interface. The results are explained in terms of Anderson localization and the position of the mobility edge with respect to the Fermi level.

DOI: 10.1103/PhysRevB.88.161107 PACS number(s): 73.40.−c, 73.20.−r, 73.21.Ac

The two-dimensional electron gas (2DEG) at the interface between the band insulators $LaAlO_3$ and $SrTiO_3$ (Ref. 1) continues to stimulate the interest of condensed matter researchers. It exhibits a variety of unexpected properties such as superconductivity,[2] magnetism,[3] spin-orbital coupling,[4] and electronic phase separation.[5–9] Recent observation of high mobility at low temperatures ($>5 \times 10^4$ cm^2 V^{-1} s^{-1})[10] and the fabrication of millions of transistors on a single chip[11] have highlighted the importance of these oxide interfaces both from fundamental and applied perspectives. The 2DEG is thought to result from an electron transfer to the interface between the polar oxide ($LaAlO_3$) and the nonpolar oxide ($SrTiO_3$), which is necessary to avoid a divergence of the energy associated with the electric field.[12] A charge transfer of 0.5 electrons per interface unit cell (uc) or 3.3×10^{14} cm^{-2} should be required to compensate the electric field in polar $LaAlO_3$ and avert a polar catastrophe.[12] However, a major puzzle is that the experimentally observed carrier densities at low temperatures for the 2DEG in fully oxidized samples[3,5,13] are an order of magnitude lower than expected. Furthermore, it is unclear where exactly at the interface the conduction electrons are located, since the $LaAlO_3$ is usually grown on a $SrTiO_3$ substrate. One proposed explanation is that these "disappearing" electrons are localized within the first $SrTiO_3$ layers that are closest to the interface, where Ti $3d_{xy}$ subbands have lower energy than the other Ti $3d$ orbitals.[14–16] According to the theoretical calculations, the mobile electrons responsible for the transport properties of the 2DEG are farther away ($\geqslant 4$ uc) from the interface.[15] While experimental results[12,17–19] have shown that the 2DEG can penetrate some distance from the interface into the $SrTiO_3$ layer, the exact location of the conduction electrons has not been determined. Since the conventional way to fabricate $LaAlO_3/SrTiO_3$ interfaces is to grow $LaAlO_3$ layers on $SrTiO_3$ substrates, it had not been possible to determine the location of the conducting channel.

A drawback with conventional $LaAlO_3/SrTiO_3$ interfaces[1–13] is that losses in the $SrTiO_3$ substrate limit the potential application of the 2DEG in high frequency devices.[20] In order to overcome this limitation and expand the applicability of 2DEG, $LaAlO_3/SrTiO_3$ interfaces have been fabricated on other substrates such as silicon,[21] $NdGaO_3$ (110),[22] $(LaAlO_3)_{0.3}(Sr_2AlTaO_6)_{0.7}$ (001),[22–24] and $DyScO_3$ (110).[22] Such an approach may permit a demonstration of the novel *topological superconductivity* recently predicted to appear in two-layer interacting Rashba systems, which might be fabricated by growing $LaAlO_3/SrTiO_3$ interfaces on $LaAlO_3$ substrates.[25] The main aim of the present Rapid Communication is to understand how the physical properties of the 2DEG vary with the thickness of the $SrTiO_3$ layer at the interface, and to study the transport properties of the electrons involved.

We have grown a $LaAlO_3/SrTiO_3$ heterostructure on $NdGaO_3$ (110) substrates. The crystal structure of $NdGaO_3$ is indexed on an orthorhombic ($\sqrt{2}a_0,\sqrt{2}a_0,2a_0$) type cell with $a = 5.433$ Å, $b = 5.503$ Å, and $c = 7.716$ Å. When indexed on the pseudocubic cell (a_0,a_0,a_0), the in-plane lattice constants a_0 for the pseudocubic lattices of $SrTiO_3$ (100), $NdGaO_3$ (110), and $LaAlO_3$ (100) are 3.905, 3.858, and 3.790 Å, respectively. It is therefore possible to grow epitaxial $LaAlO_3/SrTiO_3$ (100) interfaces on $NdGaO_3$ (110) substrates. Ideally, a $LaAlO_3$ (100) substrate would be the best candidate due to its capacity to reduce the lattice-mismatch-induced strain at the interface, and its low loss tangent at high frequencies.[20,26] However, problems of crystal twinning[27] and unstable surface termination[28] in $LaAlO_3$ set a very stringent limit, as for using a $LaAlO_3/SrTiO_3/LaAlO_3$ structure for the observation of topological superconductivity,[25] and this leads us to choose $NdGaO_3$ (110) instead. At a conventional $LaAlO_3/SrTiO_3$ interface, the lattice mismatch between $LaAlO_3$ and $SrTiO_3$ is 3%, and it is responsible for the interface strain. However, when the $SrTiO_3$ layer

 ©2013 American Physical Society

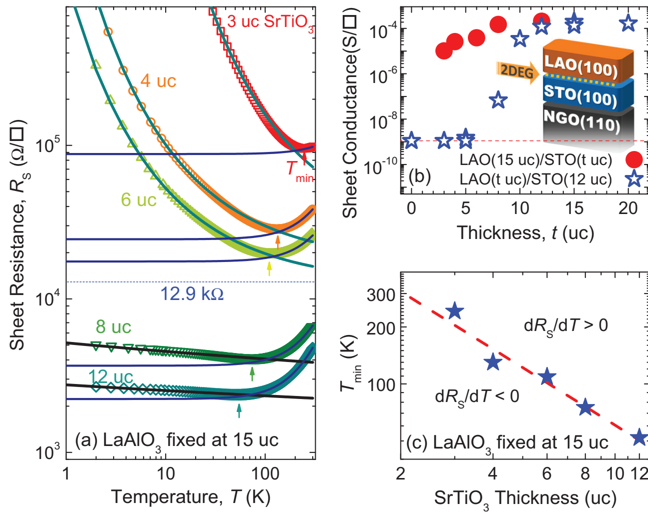

FIG. 1. (Color online) (a) R_S-T curves for $LaAlO_3/SrTiO_3/NdGaO_3$ heterostructures with fixed $LaAlO_3$ thickness (15 uc) and different $SrTiO_3$ thicknesses (from 3 to 12 uc). The blue, dark cyan, and black lines are fits using electron-electron scattering, modified VRH with a two-dimensional Coulomb gap, and weak localization models, respectively. The arrows indicate the upturn temperatures T_{min}. (b) Room-temperature sheet conductivity as a function of $LaAlO_3$ thickness for a fixed $SrTiO_3$ thickness of 12 uc, and also as a function of $SrTiO_3$ thickness for a fixed $LaAlO_3$ thickness of 15 uc. The red dashed line is the measurement limitation. The inset is the schematic view for layer structures in a $LaAlO_3/SrTiO_3/NdGaO_3$ [LAO(100)/STO(100)/NGO(110)] heterostructure, in which the 2DEG exists at the $LaAlO_3/SrTiO_3$ interface. (c) "Metal-insulator" phase diagram of $LaAlO_3/SrTiO_3/NdGaO_3$ heterostructure vs $SrTiO_3$ thickness with a fixed $LaAlO_3$ thickness of 15 uc. The slope of the red dashed line is -1.

is grown on $NdGaO_3$ (110), the large mismatch between $LaAlO_3$ and $SrTiO_3$ will be partially transferred from the $LaAlO_3/SrTiO_3$ interface to the $SrTiO_3/NdGaO_3$ interface. To investigate the depth dependence of the 2DEG, we varied the $SrTiO_3$ thickness t from 3 to 25 uc during the fabrication of $LaAlO_3/SrTiO_3/NdGaO_3$ heterostructures, which were capped with 15 uc of $LaAlO_3$ (Fig. S1 in the Supplemental Material).[29] Before deposition, the $NdGaO_3$ substrates were annealed at 1050 °C in air for 2.5 h to obtain the atomically flat B-site terminated surfaces.[30] The growth parameters for both $SrTiO_3$ and $LaAlO_3$ layers are as follows: 1.8 J/cm^2 for laser energy, 760 °C for temperature, and 2×10^{-4} Torr for oxygen partial pressure during the deposition.

The results on temperature-dependent sheet resistance (R_S-T) are shown in Fig. 1(a). Although at high temperatures the resistance of all the $LaAlO_3/SrTiO_3/NdGaO_3$ samples is dominated by electron-electron scattering with an $R_S \propto T^2$, an upturn of sheet resistance invariably occurs below a temperature T_{min} (where R_S is minimum). This upturn in R_S-T has been also reported at $LaAlO_3/SrTiO_3$ interfaces grown on other substrates,[21,23,24] and it depends on the stoichiometry of $LaAlO_3$.[31] Reducing the thickness of the $SrTiO_3$ layer raises T_{min} and R_S at the same time. For the samples with 3, 4, and 6 uc $SrTiO_3$ layers, the R_S at 2 K is far above the quantum of resistance (12.9 kΩ, including spin degeneracy). The R_S-T curves for these samples diverge as the temperature is decreased, and they can be well fitted to $R_S \propto \exp[(T_0/T)^{1/2}]$, which suggests carrier localization in these heterostructures and modified variable-range hopping (VRH) with a soft two-dimensional Coulomb gap.[32] For comparison, the samples with a thicker $SrTiO_3$ (8 and 12 uc) have R_S less than half of 12.9 kΩ, and the R_S-T curves are of the form $1/R_S \propto A + B \ln T$ (A and B are constants) below T_{min}, suggesting weak localization in two dimensions.[33] Given our experimental result that the $SrTiO_3/NdGaO_3$ heterostructures prepared in 10^{-4} Torr are insulating ($R_S > 10^7$ Ω), the conducting behavior ($dR_S/dT > 0$ and only weak localization at low temperatures) seen in Fig. 1(a) must be due to the electrons at the $LaAlO_3/SrTiO_3$ interface.

This insulating $SrTiO_3/NdGaO_3$ interface is different from the conducting one, which is found when $NdGaO_3$ is grown on a $SrTiO_3$ substrate.[34] In the former case, there is no observable conductivity, similar to the insulating interface, where the $SrTiO_3$ layers are grown on a $LaAlO_3$ substrate.[35] This can be ascribed to the loss of polar discontinuity at the interface. When $NdGaO_3$ or $LaAlO_3$ is not a freshly deposited polar layer, but the substrate itself which has been exposed to the ambient atmosphere, the surface charge is compensated by some external charge centers, as the surface of the $NdGaO_3$ or $LaAlO_3$ substrate becomes neutral. Hence, the polar discontinuity cannot be easily established at the interface when polar oxides are used as substrates. Similar results to those in Fig. 1(a) are observed when the $NdGaO_3$ (110) substrates are replaced by $(LaAlO_3)_{0.3}(Sr_2AlTaO_6)_{0.7}$ (001), which shows that a band-gap mismatch with the substrate is not a critical factor.

Moreover, the conducting behavior of the $LaAlO_3/SrTiO_3/NdGaO_3$ samples also depends greatly on the $LaAlO_3$ thickness, as shown in Fig. 1(b), where it is seen that 10–12 uc of $LaAlO_3$ are needed to make 12 uc of $SrTiO_3$ conducting. But this critical thickness of $LaAlO_3$ is larger than 4 uc that are commonly observed at conventional $LaAlO_3/SrTiO_3$ interfaces. Given that a higher critical thickness for the $LaAlO_3/SrTiO_3$ interfaces grown on other substrates is also observed by Bark *et al.*, who found that with 50 uc $SrTiO_3$ the critical $LaAlO_3$ thickness is around 15 uc,[22] this result could imply an important role of the strain in this phenomenon. Figure 1(c) shows the variation of T_{min} with $SrTiO_3$ thickness t. The temperature T_{min} separates the regions with $dR_S/dT > 0$ for the higher temperatures and thicker $SrTiO_3$ layers, and $dR_S/dT < 0$ on the opposite side. The dependence of T_{min} on $SrTiO_3$ thickness can be described by $T_{min} \sim 1/t$, which is consistent with a temperature-dependent mean free path or relaxation time signifying small energy transfer scattering in the 2DEG.[36–38]

The temperature dependence of sheet carrier density (n_S) and mobility (μ_H) are plotted in Figs. 2(a) and 2(b), respectively. Compared to conventional $LaAlO_3/SrTiO_3$ interfaces grown on $SrTiO_3$ substrates,[3,5] the interfaces grown epitaxially on $NdGaO_3$ with an 8–16 uc $SrTiO_3$ layer show an n_S independent of temperature below 100 K that is one order of magnitude larger, and close to the value of 3.3×10^{14} cm^{-2}, which corresponds to 0.5 electrons per unit cell at the interface. It can be argued that the reason for the temperature independence is the clamping effect of the $NdGaO_3$ substrate,

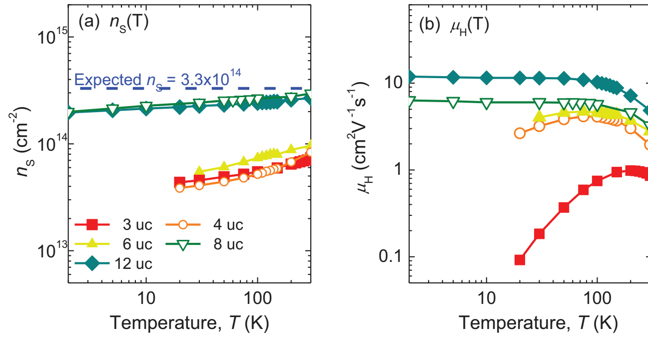

FIG. 2. (Color online) (a) The carrier density n_S and (b) mobility μ_H as a function of temperature for samples with different $SrTiO_3$ thicknesses, from 3 to 12 uc, keeping the $LaAlO_3$ thickness at 15 uc.

which prevents the $SrTiO_3$ layer from undergoing the structural transitions that occur at low temperatures,[5,39] thus avoiding the strong localization of carriers at low temperatures, which is widely observed in the 2DEG on $SrTiO_3$ substrates. This result supports the view that the $SrTiO_3$ phase transitions are important for determining the low temperature 2DEG properties, carrier localization in particular.[40] Also the absence of temperature dependence in mobility when the free carrier concentration is high suggests that electron-electron scattering is dominant. The main point here is that these characteristics, the temperature-independent value of n_S and the high density of free carriers approaching the ideal value predicted by the polar catastrophe model, are observed only when the number of $SrTiO_3$ monolayers is $\geqslant 8$. This implies that the formation of a mobile 2DEG requires at least 8 uc ($\sim$3 nm) of $SrTiO_3$ for the conducting channel, which should be regarded as the minimal propagating depth for the 2DEG and is consistent with previous experiments performed on conventional $LaAlO_3/SrTiO_3$ heterostructures,[12,17] but this time the opposite limit, i.e., carrier localization induced in $SrTiO_3$ layers $\leqslant$6 uc thick, has been directly observed.

In order to illustrate further the effect of $SrTiO_3$ thickness on the 2DEG, room-temperature n_S and μ_H as a function of $SrTiO_3$ thickness t are plotted in Figs. 3(a) and 3(b). The abrupt enhancement of n_S from 0.9×10^{14} to 2.9×10^{14} cm^{-2} is observed in a very small window of $SrTiO_3$ thicknesses, i.e., from 6 to 8 uc. The value of n_S seems to saturate for $t =$ 8–16 uc, and then falls to 0.8×10^{14} and 0.6×10^{14} cm^{-2} at 20 and 25 uc. This is also consistent with the results of Bark *et al.*, who observed a low value of $n_S = 0.5 \times 10^{14}$ cm^{-2} at 50 uc.[22] On the other hand, in Fig. 3(b), a linear increase of room-temperature μ_H with $SrTiO_3$ thickness is observed from 3 to 12 uc, which proves that the $SrTiO_3$ layer is truly the conducting channel for the 2DEG. On further increasing the $SrTiO_3$ thickness to 16 and 25 uc, a nearly constant μ_H (close to that for the conventional $LaAlO_3/SrTiO_3$ interface at room temperature) is attained. According to the above data, the $SrTiO_3$ thickness required for a mobile 2DEG is around 8–16 uc.

A rough estimate of the width t of the 2DEG at the interface can be obtained by considering its energy per unit area [Fig. 3(c), and Fig. S9 in the Supplemental Material].[41] Generally, the electrons can lower their energy by spreading out deeper into the $SrTiO_3$, provided the states are available.

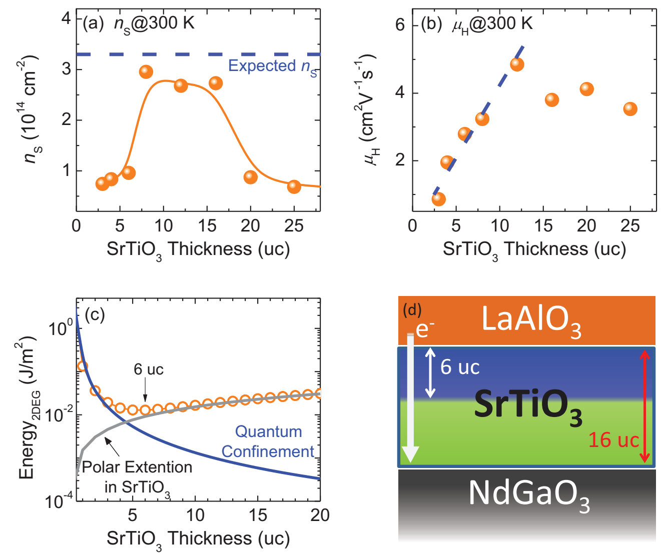

FIG. 3. (Color online) The $SrTiO_3$ thickness-dependent n_S and μ_H at 300 K are shown in (a) and (b), respectively. (c) The calculation of 2DEG energy per unit area of interface. (d) Schematic view of the $LaAlO_3/SrTiO_3/NdGaO_3$ heterostructure showing at low temperatures the $SrTiO_3$ thickness range for a mobile 2DEG is around 8–16 uc (green area), and below 6 uc the carriers are localized (blue area).

However, there is an energy penalty to be paid because the polarization fields extend into the $SrTiO_3$, hence the total energy to confine the 2DEG in $SrTiO_3$ can be written as

$$E_{2DEG} \approx n\hbar^2/2mt^2 + \sigma^2 t/24\varepsilon_0\varepsilon, \quad (1)$$

where n is the electron density per unit area, m is the electron mass, σ is the sheet charge density, and ε is the dielectric constant of $SrTiO_3$. Minimizing this energy with respect to t, we find the minimum at

$$t = [24\varepsilon_0\varepsilon n\hbar^2/m\sigma^2]^{1/3}, \quad (2)$$

with $n = 3.3 \times 10^{14}$ cm^{-2}, $\sigma = 50\ \mu$C cm^{-2}, and $\varepsilon = 300$, a value that depends little on temperature in $SrTiO_3$ thin films,[42] and this gives us a $SrTiO_3$ thickness of 2.2 nm or 6 uc, which is close to our minimal $SrTiO_3$ thickness of 8 uc for a delocalized 2DEG.

We propose that the electron transport is dominated by Anderson localization, which is related to the two-dimensional nature of the channel. The delocalized carrier density depends on the effective position of the mobility edge (E_M) with respect to the Fermi level (E_F). When the $SrTiO_3$ layer is very thin, the electrons are localized because of the potential fluctuations induced by charge disorder due to ionic interdiffusion at the interface. This ionic interdiffusion usually involves the first 1–2 uc from the interface, and it will create a mobility edge, localizing the states at the bottom of the band. As the $SrTiO_3$ thickness increases, these potential fluctuations are screened, and the mobility edge drops rapidly to a lower energy. The Fermi energy falls less rapidly with thickness, varying as $1/t$ for a constant density of states. At about 8 uc of $SrTiO_3$, E_F exceeds E_M and we see the onset of electron delocalization, and metallic conductivity at low temperatures. Our experiments clearly prove that the conducting electrons are

located appreciably below the $LaAlO_3/SrTiO_3$ interface of our films. The reduction in carrier density again in $SrTiO_3$ layers thicker than 16 uc could be understood in several ways. As the 0.5 electrons per Ti extend into $SrTiO_3$ layer farther from the interface, the Fermi level E_F falls towards the bottom of the band due to the increase of available electronic states and it approaches the t_{2g} band mobility edge for the bulk. This arises from defects such as oxygen vacancies that are distributed throughout the $SrTiO_3$, which is more disordered when it is an epitaxially grown layer rather than a single-crystal substrate. Also, there is a tendency for strain relaxation and associated defect production in these thicker $SrTiO_3$ layers, which can raise the mobility edge again and localize the carriers. A third possibility is the polarization of the distorted $SrTiO_3$ layer, which can compensate the polarization catastrophe at the interface.[22]

We can model the number of mobile electrons with thickness quite nicely with a single band having a constant density of states. The total number of available states increases in proportion to the number of layers, leading to a Fermi level (relative to the bottom of the rectangular conduction band)

$$E_F = a/t, \tag{3}$$

where t is the $SrTiO_3$ thickness and a is a constant. Then we model the mobility edge to vary due to two effects—one falling off exponentially with t, due to the disorder in the interface layer, and the other a constant low-energy mobility edge due to residual disorder in the $SrTiO_3$, giving

$$E_M = b\exp(-t/t_0) + c, \tag{4}$$

where b, t_0, and c are all constants. At room temperature, we roughly assume that there is a baseline for the delocalized carrier density n_S due to the thermal activation. Hence, n_S can be evaluated by

$$n_S(E_F) = \begin{cases} d & (E_F < E_M), \\ d + n\left[\frac{E_F - E_M}{E_F}\right] & (E_F \geqslant E_F), \end{cases} \tag{5}$$

where d is a constant baseline [assumed to be 0.5×10^{14} cm^{-2}, which is the carrier density for 50 uc $SrTiO_3$ (Ref. 22)] and n is the carrier density for the ideal 2DEG, 3.3×10^{14} cm^{-2}. Based on these, we show the fit to both E_F and E_M as a function of thickness in Fig. 4(a). Because E_F falls much more slowly with thickness and E_M is higher than E_F at low thickness, there are two crossover points of t_1 and t_2, indicating free carriers in the thickness range $t_1 < t < t_2$. The fitted curve for the delocalized carriers is also quite consistent with the experimentally observed values in Fig. 4(b). A reasonable screening length t_0 of about 1–2 unit cells is seen for the mobility edge, the details are of which is given in Fig. S10 in the Supplemental Material.[43]

In conclusion, we have shown that the thickness of the $SrTiO_3$ layer in epitaxially grown $LaAlO_3/SrTiO_3$ heterostructures is critical for determining the 2DEG transport properties. Samples with the thinnest $SrTiO_3$ exhibit a low carrier density at room temperature, a robust insulating ground state, and modified variable-range hopping transport behavior at low temperatures, due to the Anderson localization of the 2DEG arising from the random interface potential with ionic interdiffusion. When the $SrTiO_3$ thickness reaches 8–16 uc, the carrier density increases to almost the expected 0.5 electrons per interface Ti site, and the mobility saturates at the conventional room-temperature value. However, the carrier density falls again for the thicker layers to the conventional value found for single-crystal $SrTiO_3$ substrates. Most of the Ti 3d electrons are localized at the very bottom of the 3d band, below the mobility edge. We are therefore able to explain the observed behavior on a localization model where the position of the Fermi level and the mobility edge depend on the $SrTiO_3$ layer thickness. The study of these thin epitaxially grown layers has enabled us to describe the role of localization and to define the extent of the conducting region at the $LaAlO_3/SrTiO_3$ interface. It shows how to tailor the oxide interface to optimize the two-dimensional conduction, which will be of importance for oxide electronics.

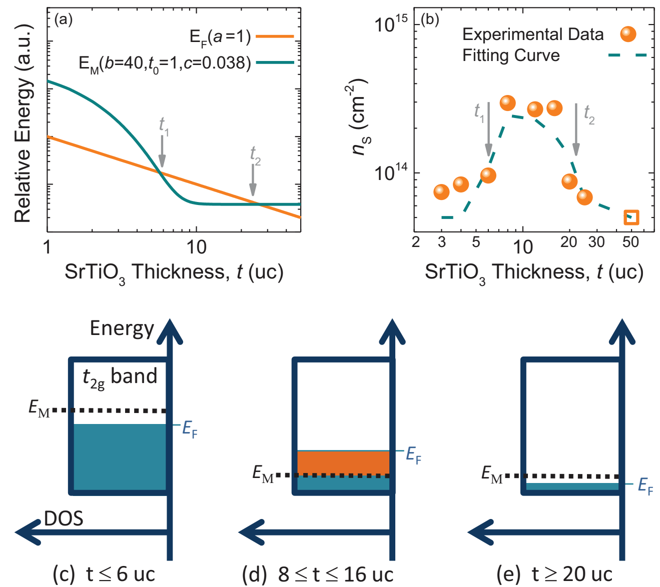

FIG. 4. (Color online) (a) Fitted E_F and E_M as a function of $SrTiO_3$ thickness. (b) The comparison on experimentally observed n_S and fitted n_S as a function of $SrTiO_3$ thickness. The open square in (b) is taken from Ref. 20 as a comparison. The details on controlling the fitting parameters are discussed in Fig. S10 (Ref. 43). Schematic 2D-density of states (DOS) (number of available electronic states per unit interface area) vs energy for the t_{2g} band are shown with $SrTiO_3$ thickness $\leqslant$6 uc in (c), 8–16 uc in (d), and $\geqslant$20 uc in (e). Electrons below E_M are localized and denoted by blue, while electrons which are below E_F but beyond E_M are delocalized and denoted by orange. In these sketches, the total area below E_F is fixed for each thickness, indicating the total number of carriers at the $LaAlO_3/SrTiO_3$ interface is fixed.

This work was financially supported by the National Research Foundation (NRF) Singapore under the Competitive Research Program "Tailoring Oxide Electronics by Atomic Control: Oxides with Novel Functionality" (R-398-000-062-281), NUS cross-faculty grant, and FRC.

*ariando@nus.edu.sg

[1] A. Ohtomo and H. Y. Hwang, Nature (London) **427**, 423 (2004).

[2] N. Reyren, S. Thiel, A. D. Caviglia, L. F. Kourkoutis, G. Hammerl, C. Richter, C. W. Schneider, T. Kopp, A.-S. Rüetschi, D. Jaccard, M. Gabay, D. A. Muller, J.-M. Triscone, and J. Mannhart, Science **317**, 1196 (2007).

[3] A. Brinkman, M. Huijben, M. van Zalk, J. Huijben, U. Zeitler, J. C. Maan, W. G. van der Wiel, G. Rijnders, D. H. A. Blank, and H. Hilgenkamp, Nat. Mater. **6**, 493 (2007).

[4] A. D. Caviglia, M. Gabay, S. Gariglio, N. Reyren, C. Cancellieri, and J.-M. Triscone, Phys. Rev. Lett. **104**, 126803 (2010); M. Ben Shalom, M. Sachs, D. Rakhmilevitch, A. Palevski, and Y. Dagan, *ibid.* **104**, 126802 (2010).

[5] Ariando, X. Wang, G. Baskaran, Z. Q. Liu, J. Huijben, J. B. Yi, A. Annadi, A. Roy Barman, A. Rusydi, S. Dhar, Y. P. Feng, J. Ding, H. Hilgenkamp, and T. Venkatesan, Nat. Commun. **2**, 188 (2011).

[6] D. A. Dikin, M. Mehta, C. W. Bark, C. M. Folkman, C. B. Eom, and V. Chandrasekhar, Phys. Rev. Lett. **107**, 056802 (2011).

[7] J. A. Bert, B. Kalisky, C. Bell, M. Kim, Y. Hikita, H. Y. Hwang, and K. A. Moler, Nat. Phys. **7**, 767 (2011).

[8] B. Kalisky, J. A. Bert, B. B. Klopfer, C. Bell, H. K. Sato, M. Hosoda, Y. Hikita, H. Y. Hwang, and K. A. Moler, Nat. Commun. **3**, 922 (2012).

[9] L. Li, C. Richter, J. Mannhart, and R. C. Ashoori, Nat. Phys. **7**, 762 (2011).

[10] M. Huijben, G. Koster, M. K. Kruize, S. Wenderich, J. Verbeeck, S. Bals, E. Slooten, B. Shi, H. J. A. Molegraaf, J. E. Kleibeuker, S. van Aert, J. B. Goedkoop, A. Brinkman, D. H. A. Blank, M. S. Golden, G. van Tendeloo, H. Hilgenkamp, and G. Rijnders, Adv. Funct. Mater., doi: 10.1002/adfm.201203355 (2013).

[11] B. Förg, C. Richter, and J. Mannhart, Appl. Phys. Lett. **100**, 053506 (2012).

[12] N. Nakagawa, H. Y. Hwang, and D. A. Muller, Nat. Mater. **5**, 204 (2006).

[13] C. Cancellieri, N. Reyren, S. Gariglio, A. D. Caviglia, A. Fête, and J.-M. Triscone, Europhys. Lett. **91**, 17004 (2010).

[14] Z. S. Popović, S. Satpathy, and R. M. Martin, Phys. Rev. Lett. **101**, 256801 (2008).

[15] P. Delugas, A. Filippetti, V. Fiorentini, D. I. Bilc, D. Fontaine, and P. Ghosez, Phys. Rev. Lett. **106**, 166807 (2011).

[16] M. Salluzzo, J. C. Cezar, N. B. Brookes, V. Bisogni, G. M. De Luca, C. Richter, S. Thiel, J. Mannhart, M. Huijben, A. Brinkman, G. Rijnders, and G. Ghiringhelli, Phys. Rev. Lett. **102**, 166804 (2009).

[17] M. Basletic, J.-L. Maurice, C. Carrétéro, G. Herranz, O. Copie, M. Bibes, É. Jacquet, K. Bouzehouane, S. Fusil, and A. Barthélémy, Nat. Mater. **7**, 621 (2008).

[18] O. Copie, V. Garcia, C. Bödefeld, C. Carrétéro, M. Bibes, G. Herranz, E. Jacquet, J.-L. Maurice, B. Vinter, S. Fusil, K. Bouzehouane, H. Jaffrès, and A. Barthélémy, Phys. Rev. Lett. **102**, 216804 (2009).

[19] T. Fix, J. L. MacManus-Driscoll, and M. G. Blamire, Appl. Phys. Lett. **94**, 172101 (2009).

[20] J. M. Phillips, J. Appl. Phys. **79**, 1829 (1996).

[21] J. W. Park, D. F. Bogorin, C. Cen, D. A. Felker, Y. Zhang, C. T. Nelson, C. W. Bark, C. M. Folkman, X. Q. Pan, M. S. Rzchowski, J. Levy, and C. B. Eom, Nat. Commun. **1**, 94 (2010).

[22] C. W. Bark, D. A. Felker, Y. Wang, Y. Zhang, H. W. Jang, C. M. Folkman, J. W. Park, S. H. Baek, H. Zhou, D. D. Fong, X. Q. Pan, E. Y. Tsymbal, M. S. Rzchowski, and C. B. Eom, Proc. Natl. Acad. Sci. USA **108**, 4720 (2011).

[23] P. Brinks, W. Siemons, J. E. Kleibeuker, G. Koster, G. Rijnders, and M. Huijben, Appl. Phys. Lett. **98**, 242904 (2011).

[24] T. Hernandez, C. W. Bark, D. A. Felker, C. B. Eom, and M. S. Rzchowski, Phys. Rev. B **85**, 161407 (2012).

[25] S. Nakosai, Y. Tanaka, and N. Nagaosa, Phys. Rev. Lett. **108**, 147003 (2012).

[26] C. Zuccaro, M. Winter, N. Klein, and K. Urban, J. Appl. Phys. **82**, 5695 (1997).

[27] Z. L. Wang and A. J. Shapiro, Surf. Sci. **328**, 141 (1995).

[28] J. Yao, P. B. Merrill, S. S. Perry, D. Marton, and J. W. Rabalais, J. Chem. Phys. **108**, 1645 (1998).

[29] See Supplemental Material at http://link.aps.org/supplemental/10.1103/PhysRevB.88.161107 for detailed interface growth conditions and characterization.

[30] R. Gunnarsson, A. S. Kalabukhov, and D. Winkler, Surf. Sci. **603**, 151 (2009).

[31] E. Breckenfeld, N. Bronn, J. Karthik, A. R. Damodaran, S. Lee, N. Mason, and L. W. Martin, Phys. Rev. Lett. **110**, 196804 (2013).

[32] V. Yu. Butko, J. F. DiTusa, and P. W. Adams, Phys. Rev. Lett. **84**, 1543 (2000).

[33] P. A. Lee and T. V. Ramakrishnan, Rev. Mod. Phys. **57**, 287 (1985); A. D. Caviglia, S. Gariglio, N. Reyren, D. Jaccard, T. Schneider, M. Gabay, S. Thiel, G. Hammerl, J. Mannhart, and J.-M. Triscone, Nature (London) **456**, 624 (2008).

[34] A. Annadi, A. Putra, Z. Q. Liu, X. Wang, K. Gopinadhan, Z. Huang, S. Dhar, T. Venkatesan, and Ariando, Phys. Rev. B **86**, 085450 (2012); U. S. di Uccio, C. Aruta, C. Cantoni, E. D. Gennaro, and A. Gadaleta, arXiv:1206.5083.

[35] Z. Q. Liu, Z. Huang, W. M. Lü, K. Gopinadhan, X. Wang, A. Annadi, T. Venkatesan, and Ariando, AIP Adv. **2**, 012147 (2012).

[36] B. L. Altshuler, A. G. Aronov, and D. E. Khmelnitsky, J. Phys. C: Solid State Phys. **15**, 7367 (1982).

[37] B. N. Narozhny, G. Zala, and I. L. Aleiner, Phys. Rev. B **65**, 180202 (2002).

[38] I. R. Pagnossin, A. K. Meikap, A. A. Quivy, and G. M. Gusev, J. Appl. Phys. **104**, 073723 (2008).

[39] F. W. Lytle, J. Appl. Phys. **35**, 2212 (1964).

[40] W. M. Lü, X. Wang, Z. Q. Liu, S. Dhar, A. Annadi, K. Gopinadhan, A. R. Barman, H. B. Su, T. Venkatesan, and Ariando, Appl. Phys. Lett. **99**, 172103 (2011).

[41] See Supplemental Material at http://link.aps.org/supplemental/10.1103/PhysRevB.88.161107 for a detailed description of calculating the 2DEG energy.

[42] A. Walkenhorst, C. Doughty, X. X. Xi, S. N. Mao, Q. Li, T. Venkatesan, and R. Ramesh, Appl. Phys. Lett. **60**, 1744 (1992).

[43] See Supplemental Material at http://link.aps.org/supplemental/10.1103/PhysRevB.88.161107 for a detailed description of the fitting parameters for E_F and E_M.